Fig. 1.
A: responses of a typical collision-sensitive neuron to an object approaching on a direct collision course (middle) and on near-miss trajectories (x − 20: forward deviation, x + 20: backward deviation, y + 20: upward deviation, y − 20: downward deviation). Top traces: voltage changes monitoring size of the approaching objects. Bottom traces: neuronal activities to the approaching objects. ■ and □, the units eliminated for quantitative analysis. Inset: the shape of spikes of the collision-sensitive neuron. B: responses to translating objects with different sizes (trans2: 2 × 2 cm square, trans10: 10 × 10 cm square, trans20: 20 × 20 cm square). Top traces: voltage changes monitoring position of the translating objects. The 1st

upward and downward deflections represent backward and forward movements of the square, respectively. The second upward and downward deflections represent upward and downward movements of the square, respectively. Bottom traces: neuronal activities to the translating objects. C: responses to 3 other control stimuli (see methods). Top and bottom ("reversed contrast" and "recession" stimuli, respectively): the top traces show voltage changes monitoring size of an approaching and a receding object, respectively. Middle ("brightness change" stimulus): the top trace shows voltage changes monitoring brightness of a stationary square. In all 3 panels, bottom traces show neuronal activities to each control stimulus. D: responses to an object approaching on a direct collision course and responses to a translating 10 × 10 cm square with a velocity of 30, 9, and 1.5 cm/s. Top left: top and bottom traces show the size of the approaching object and neuronal activity to the stimulus as shown in A. In the remaining panels, top and bottom traces show the position of the translating object and neuronal activity to the stimuli as shown in B. This neuron responds selectively to a collision stimulus. D was obtained from different preparation than A to C.
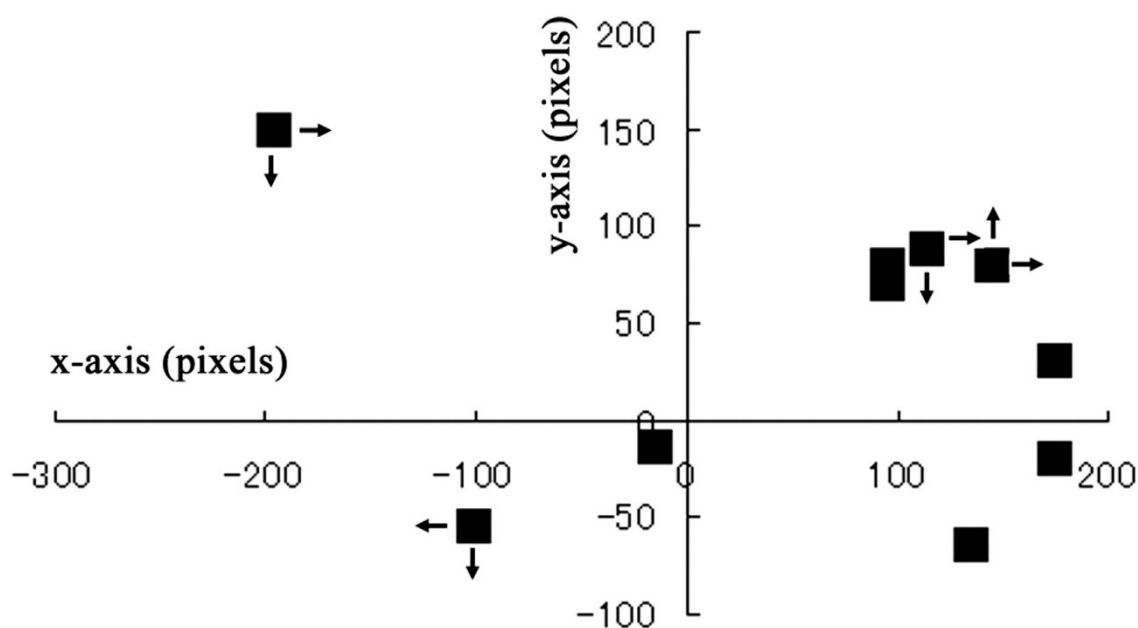
Fig. 2.

Distribution of the foci of expansion of looming stimuli that were presented to 11 collision-sensitive neurons. Seventeen pixels correspond to 1 cm on the display. The eye of the animal was aligned with y axis but located 8 cm below the origin. The arrows show the directions of horizontal and vertical deviation of the peaks of the tuning curves obtained from 4 neurons. Two data plots were completely superimposed.
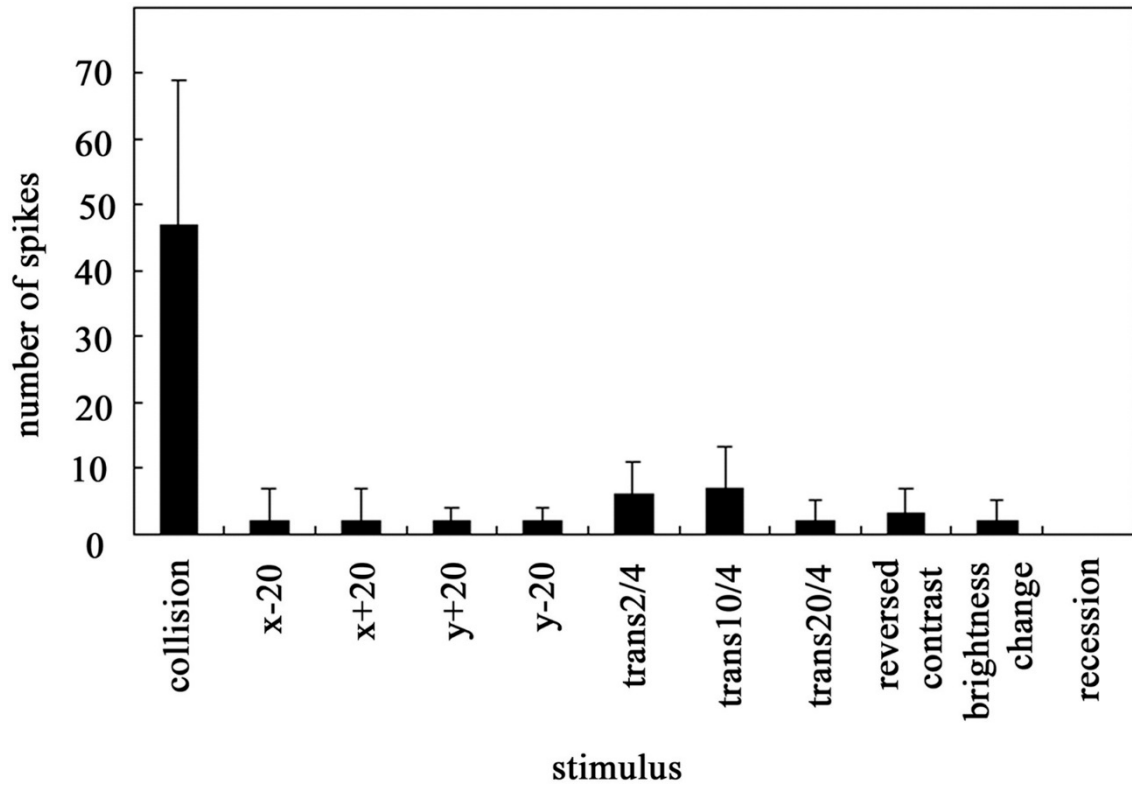
Fig. 3.

Average number of spikes (mean ± SD) per response obtained from 11 collision-sensitive neurons responding to 11 kinds of visual stimuli shown in Fig. 1. There is a significant difference between mean number of spikes for the collision stimulus and those for other stimuli (P < 0.01).
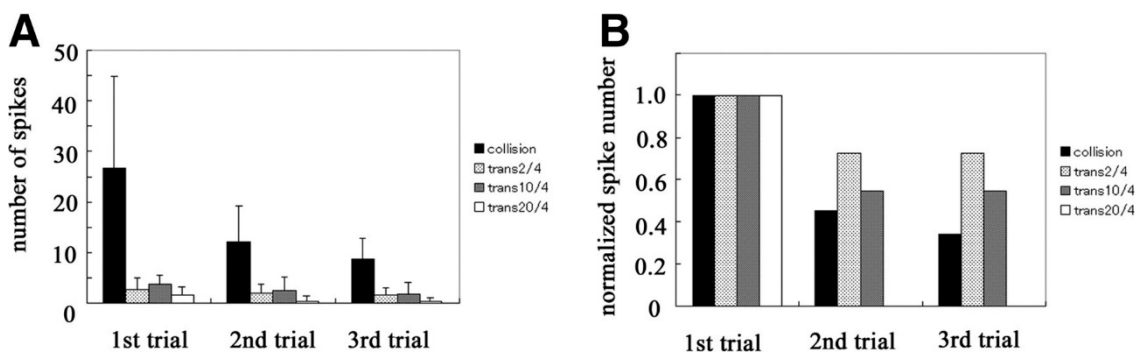
Fig. 4.

The effects of stimulus repetition on the responses of collision-sensitive neurons to an approaching object and translating objects. A: average number of spikes (mean ± SD) to 3 successive presentations of collision or translating objects obtained from 10 collision-sensitive

neurons is shown. B: the mean number of spikes to the 1st trial is normalized to 1. The responses to looming and translating objects were equally susceptible to the effects of stimulus repetition.
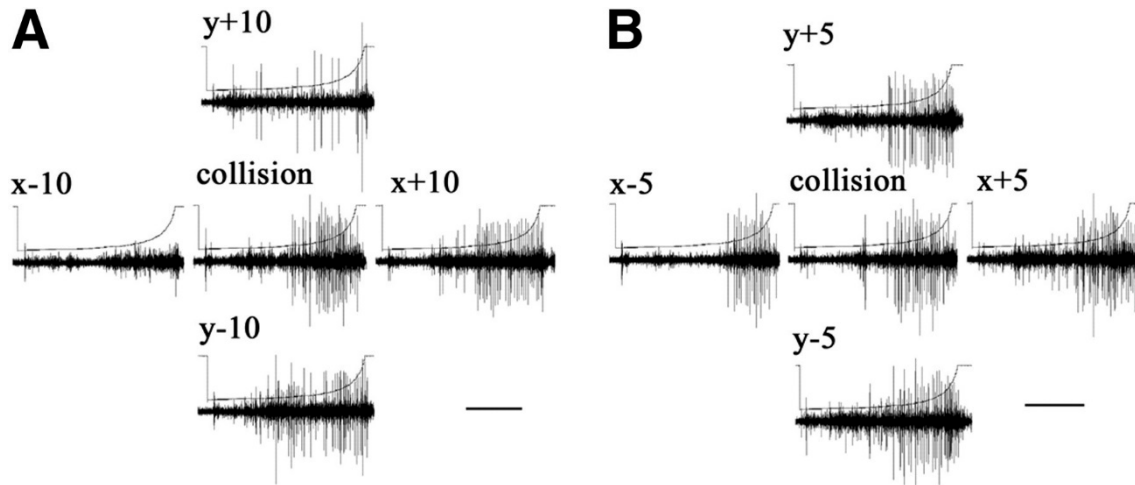
Fig. 5.

A: responses of the same neuron as in Fig. 1A–C to an object approaching on a direct collision course and near-miss trajectories with deviations from a direct collision path of 1° (x − 10: forward deviation, x + 10: backward deviation, y + 10: upward deviation, y − 10: downward deviation). B: responses of the same collision-sensitive neuron as in A to an object approaching on a direct collision course and near-miss trajectories with deviations from a direct collision path of 0.5° (x − 5: forward deviation, x + 5: backward deviation, y + 5: upward deviation, y − 5: downward deviation). Top: voltage changes monitoring size of the approaching objects. Bottom: neuronal activities to the approaching objects. Scale bars: 1 s.
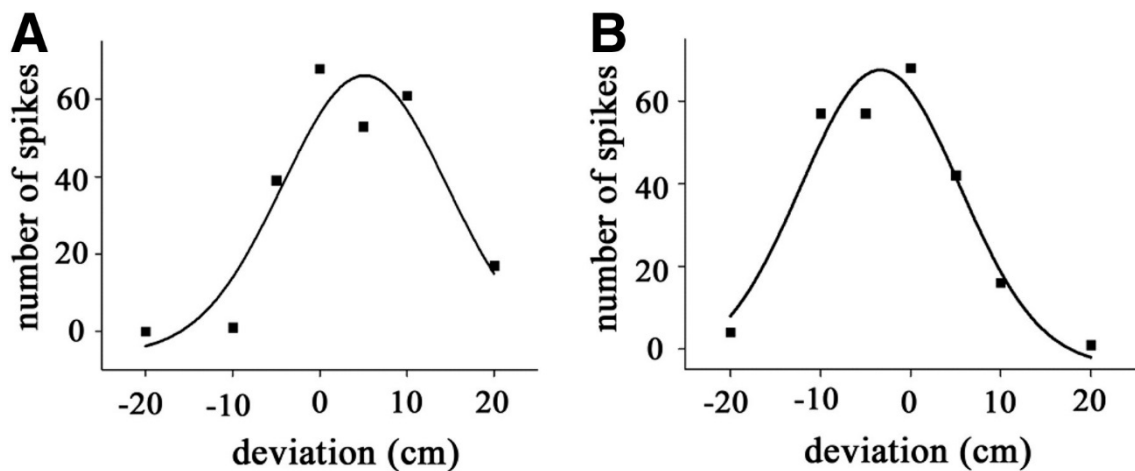
Fig. 6.

The response profiles of the same collision-sensitive neuron as in Fig. 5 to an object approaching on different trajectories and the corresponding tuning curves fitted by Gaussian function. A: total spike numbers are plotted against horizontal displacement from a direct collision path. Positive and negative displacement represents backward and forward deviation, respectively. B: total spike numbers are plotted against vertical displacement from a direct collision path. Positive and negative displacement represents upward and downward deviation, respectively.
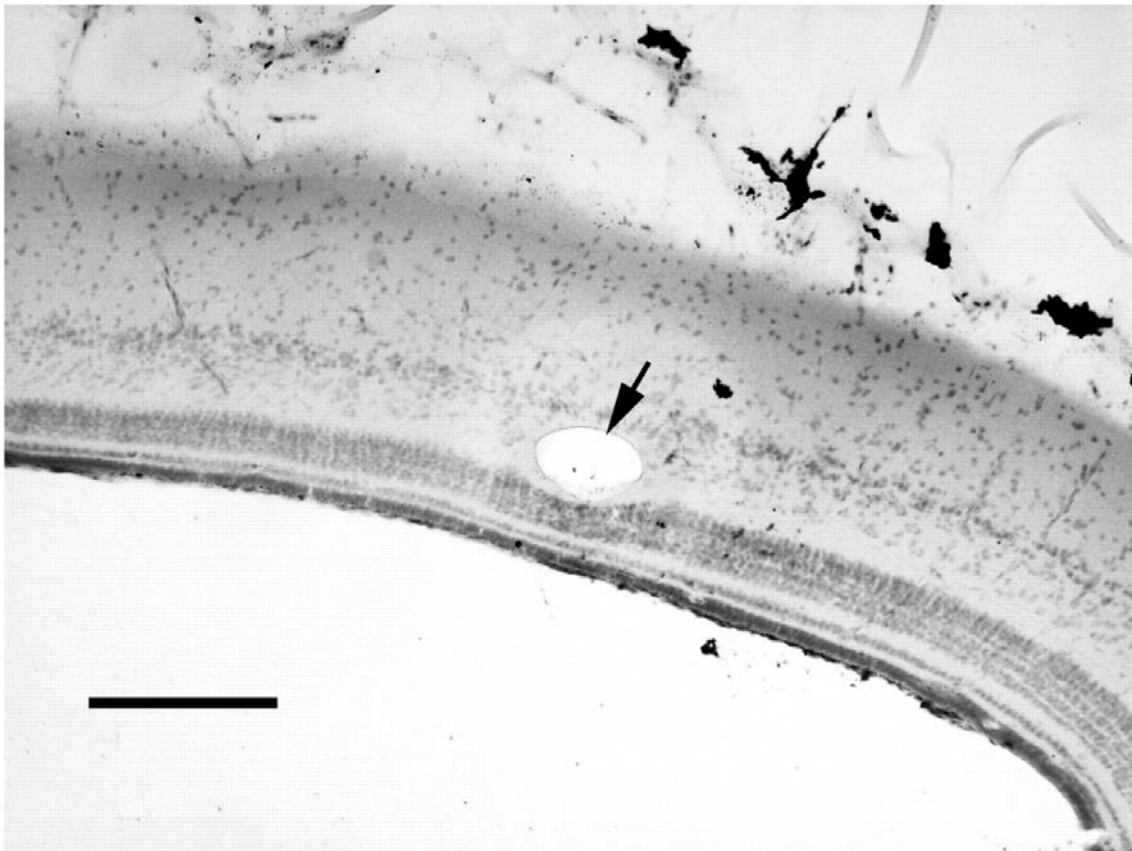
Fig. 7.
A cross section of the frog optic tectum in which a lesion of recording site was made by current injection. The lesion is observed in the tectal layer 7, the main efferent layer of the tectum (arrow). The pial surface is at the top, and the ventricular surface is at the bottom. Scale bar: 200 μm.
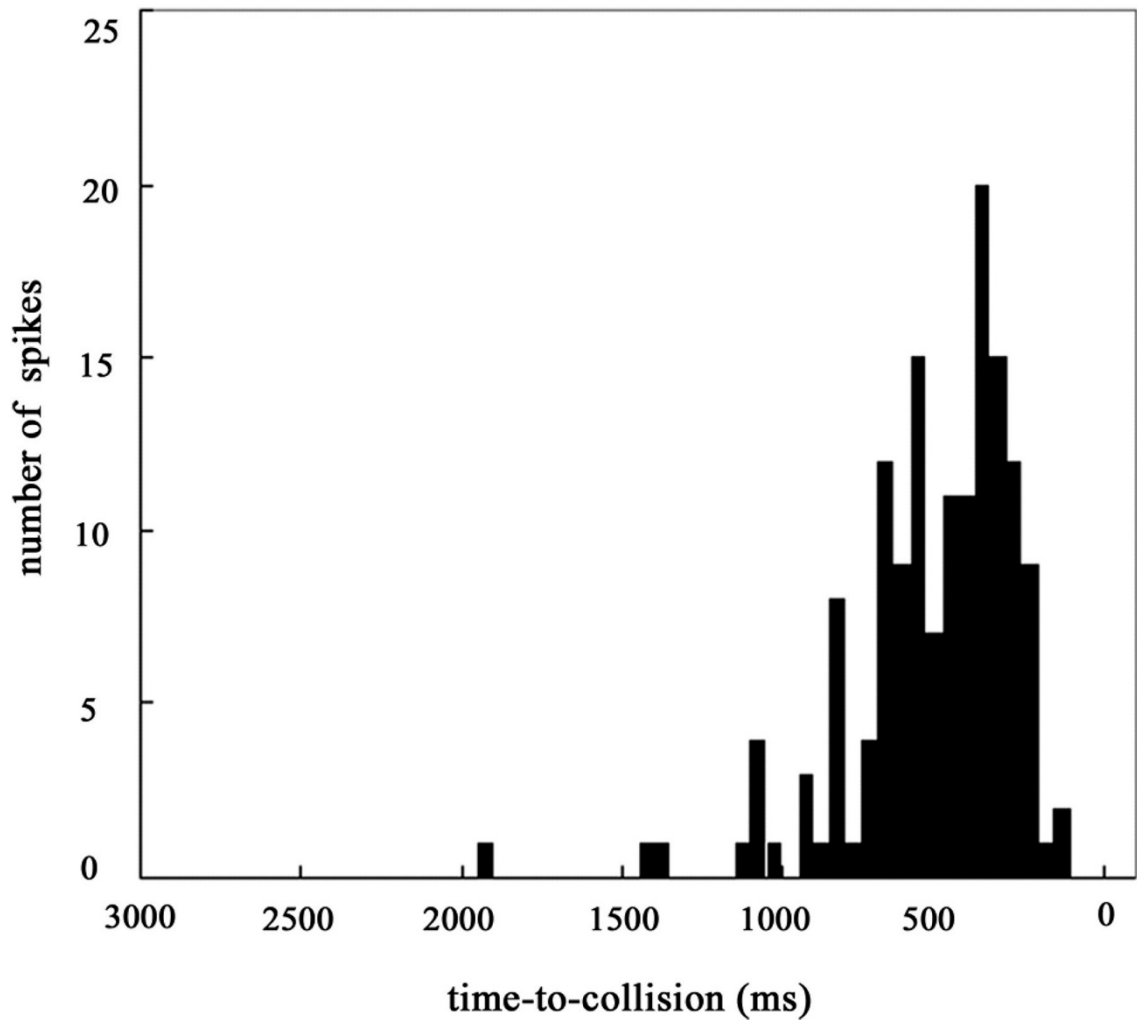
Fig. 8.

A typical response profile of a collision-sensitive neuron in response to a black square of 35 × 35 cm approaching at a velocity of 2 m/s through a direct collision path of 6 m. The number of spikes within a bin width of 50 ms was obtained from 5 blocks in which 3 successive stimuli were presented. Collision would be at 0 ms. The activity started increasing ~1 s before predictive collision. The activity peaked ~400 ms before predictive collision when the retinal image of the stimulus ranged from 25 to 28° and then declined.
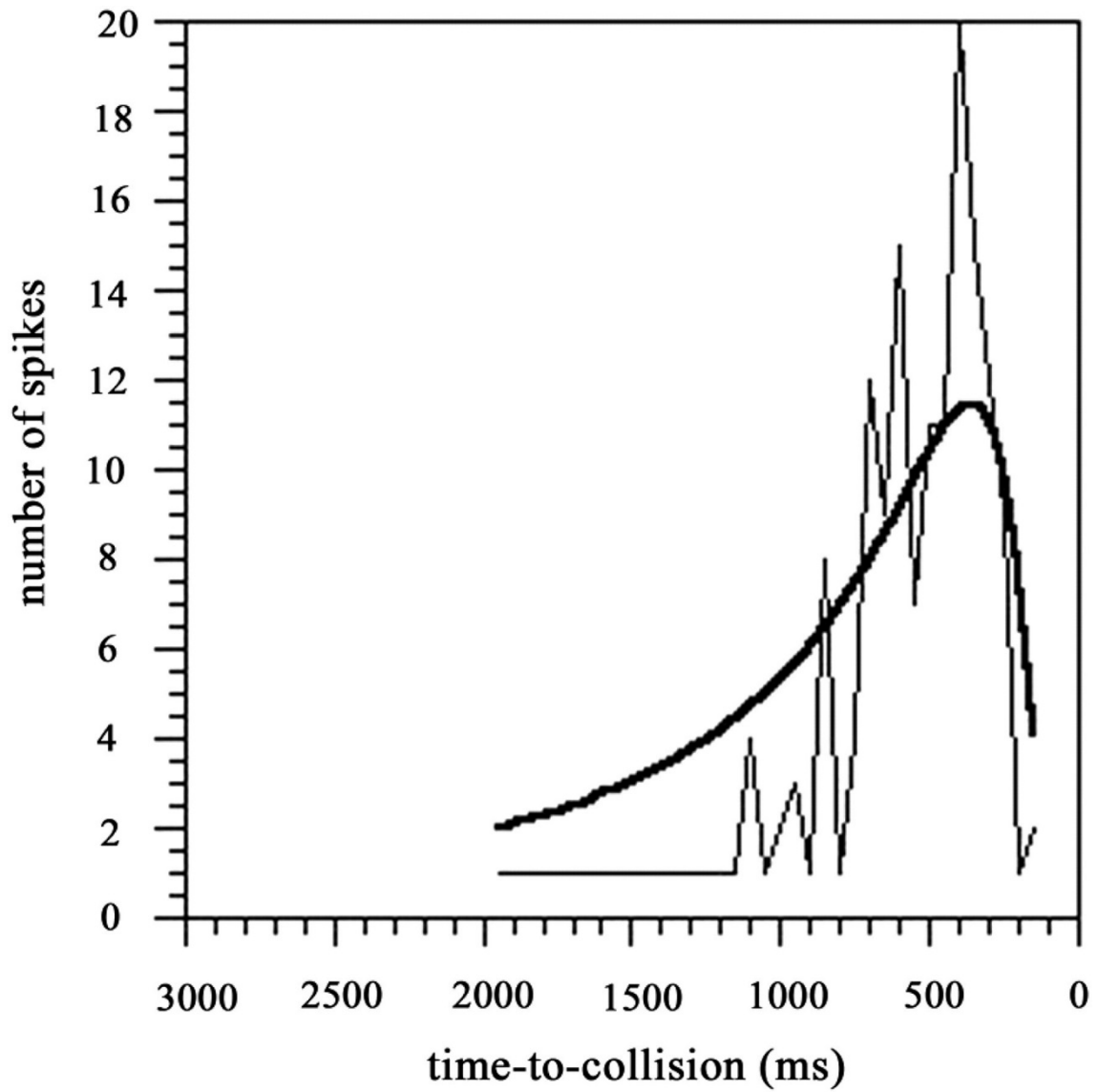
Fig. 9.

Response of the collision-sensitive neuron shown in Fig. 8 (thin line) and model prediction which is superimposed on the data (thick line). In this particular case, the response can be fitted with the equation: f(t) = 61.6 · θ' (t) · e − 4.1 θ (t). Collision would be at 0 ms.
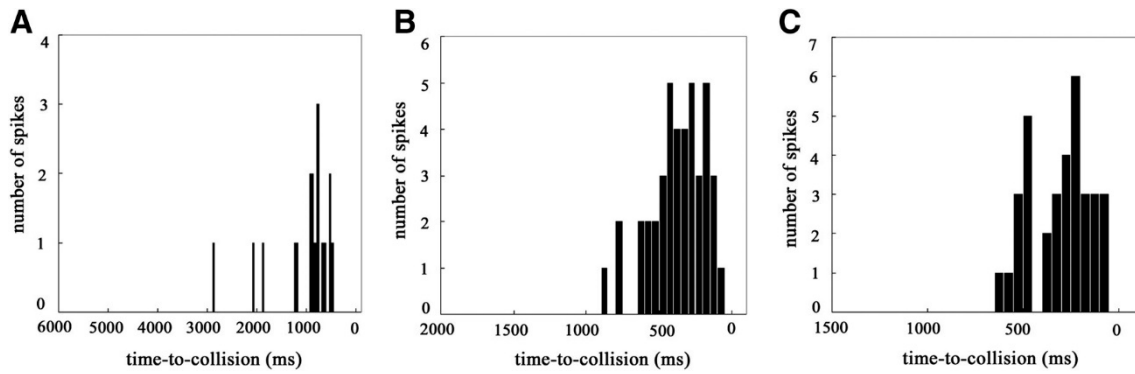
Fig. 10.

Response profiles of the same collision-sensitive neuron as in Fig. 8 in response to a black square of 35 × 35 cm approaching at a velocity of 1, 3, and 4 m/s through a direct collision path of 6 m are shown in A–C, respectively. The number of spikes within a bin width of 50 ms was calculated from 3 successive sweeps with an interval of 1 min. Collision would be at 0 ms.
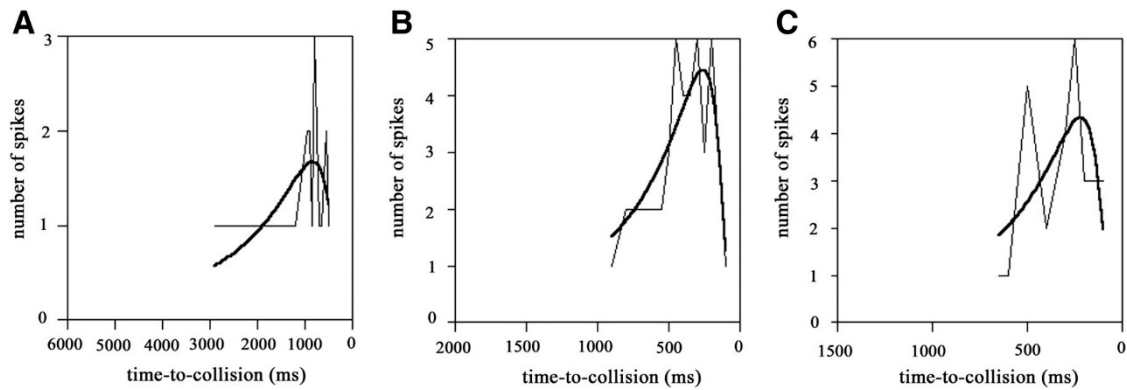
Fig. 11.

A: response of the collision-sensitive neuron shown in Fig. 10A (thin line) and model prediction that is superimposed on the data (thick line). The response can be fitted with the equation: $f(t) = 12.2 \cdot \theta'(t) \cdot e^{-4.7\theta(t)}$. B: response of the collision-sensitive neuron shown in Fig. 10B (thin line) and model prediction that is superimposed on the data (thick line). The response can be fitted with the equation: $f(t) = 27.9 \cdot \theta'(t) \cdot e^{-4.4\theta(t)}$. C: response of the collision-sensitive neuron shown in Fig. 10C (thin line) and model prediction that is superimposed on the data (thick line). The response can be fitted with the equation: $f(t) = 34.5 \cdot \theta'(t) \cdot e^{-5.0\theta(t)}$. Collision would be at 0 ms.
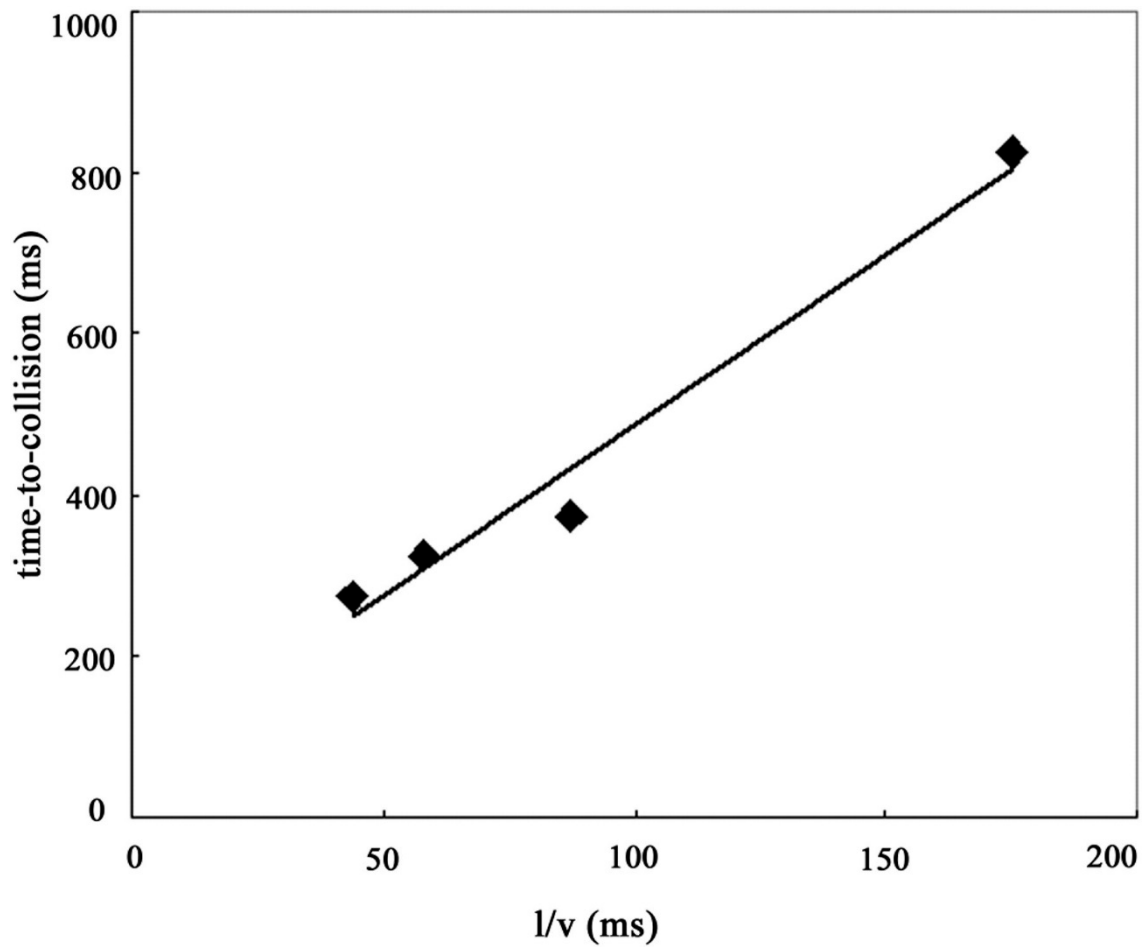
Fig. 12.

Plot of the peak time relative to the predicted collision as a function of visual parameter l/v (l: object's half size, v: approaching velocity) obtained from the same collision-sensitive neuron shown in Fig. 8. A strong linear relationship is found between the 2 parameters ($R^2 = 0.98$).
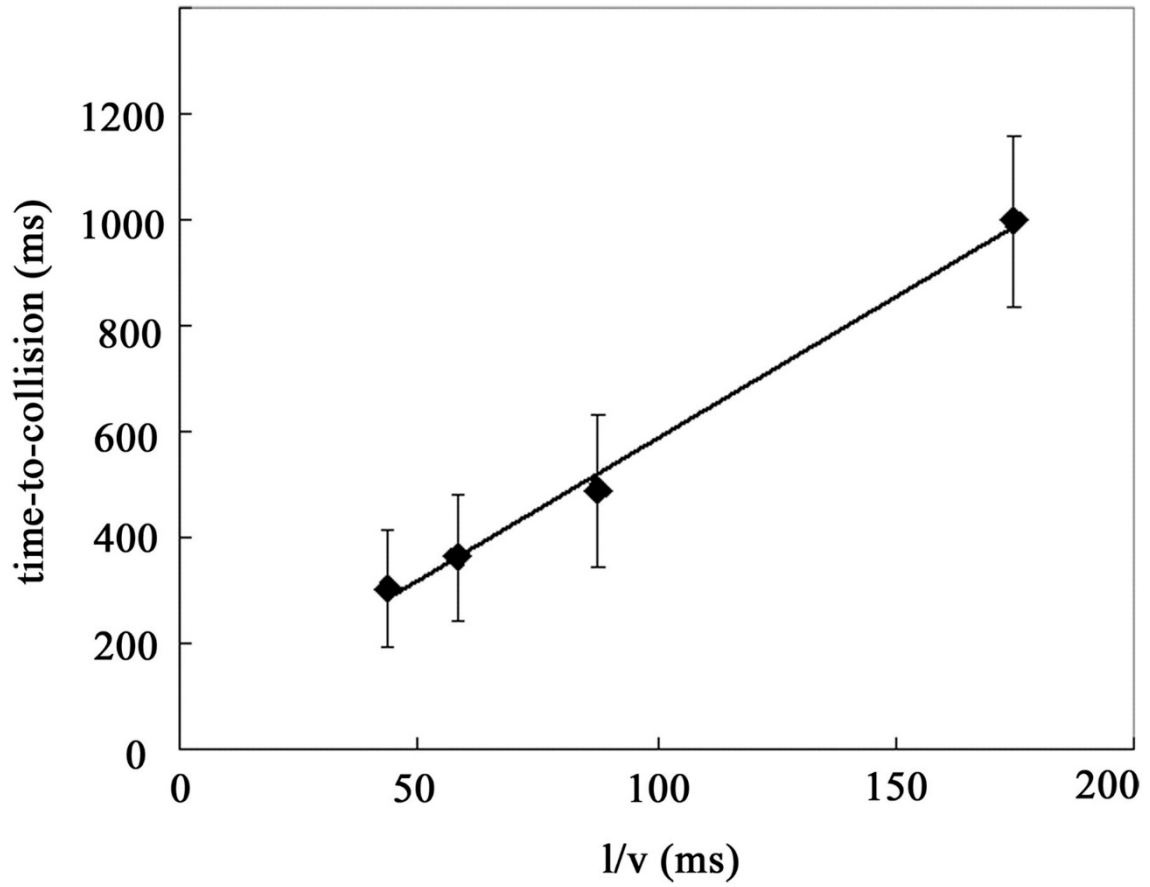
Fig. 13.

Plot of the mean peak time relative to the predicted collision as a function of visual parameter l/v (l: object's half size, v: approaching velocity) obtained from 11 collision-sensitive neurons. Error bars indicate SD. A strong linear relationship is found between the 2 parameters ($R^2 = 0.99$).
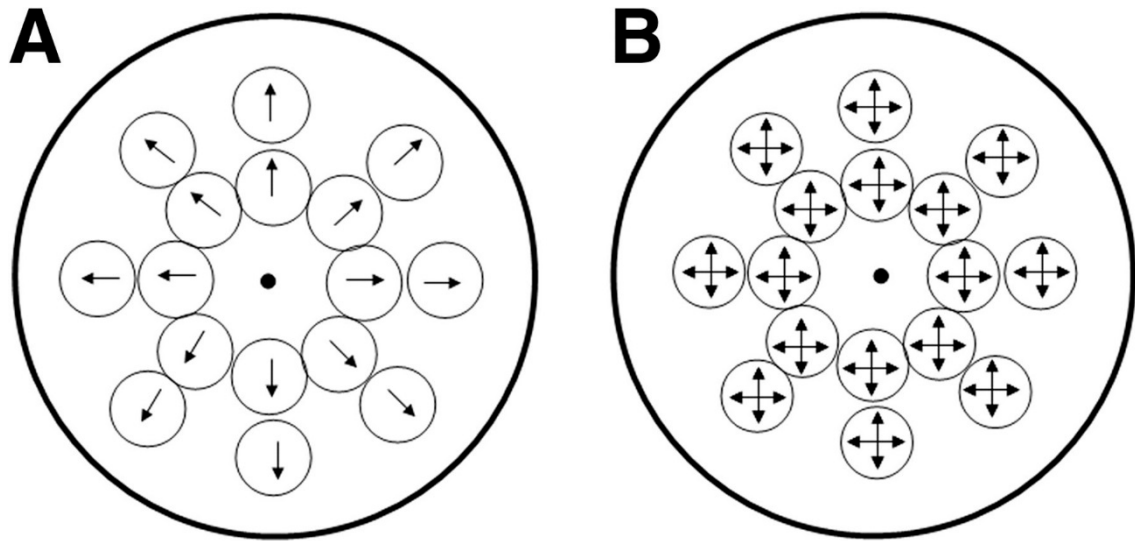
Fig. 14.

Two neuronal models to explain how tectal inputs integrate and build up the wide receptive field of thalamic collision-sensitive neurons. An outer large circle represents the receptive field of a thalamic collision-sensitive neuron. A series of concentric circles represents receptive fields of tectal neurons. A: the model proposed by Frost and Sun (2004). The tectal neurons give selective responses to movements that are oriented radially from the center of the concentric array. B: our model based on the results obtained from the present experiments. The tectal neurons respond selectively to looming stimuli that are expanded from the center of their receptive fields irrespective of the locations.